 Related Commentary, page 868

Hypoglycemic neuronal death is triggered by glucose reperfusion and activation of neuronal NADPH oxidase

Sang Won Suh,[1] Elizabeth T. Gum,[1] Aaron M. Hamby,[1] Pak H. Chan,[2] and Raymond A. Swanson[1]

[1]Department of Neurology, UCSF, and Veterans Affairs Medical Center, San Francisco, California, USA. [2]Department of Neurosurgery, Department of Neurology and Neurological Sciences, and Program in Neurosciences, Stanford University School of Medicine, Stanford, California, USA.

Hypoglycemic coma and brain injury are potential complications of insulin therapy. Certain neurons in the hippocampus and cerebral cortex are uniquely vulnerable to hypoglycemic cell death, and oxidative stress is a key event in this cell death process. Here we show that hypoglycemia-induced oxidative stress and neuronal death are attributable primarily to the activation of neuronal NADPH oxidase during glucose reperfusion. Superoxide production and neuronal death were blocked by the NADPH oxidase inhibitor apocynin in both cell culture and in vivo models of insulin-induced hypoglycemia. Superoxide production and neuronal death were also blocked in studies using mice or cultured neurons deficient in the $p47^{phox}$ subunit of NADPH oxidase. Chelation of zinc with calcium disodium EDTA blocked both the assembly of the neuronal NADPH oxidase complex and superoxide production. Inhibition of the hexose monophosphate shunt, which utilizes glucose to regenerate NADPH, also prevented superoxide formation and neuronal death, suggesting a mechanism linking glucose reperfusion to superoxide formation. Moreover, the degree of superoxide production and neuronal death increased with increasing glucose concentrations during the reperfusion period. These results suggest that high blood glucose concentrations following hypoglycemic coma can initiate neuronal death by a mechanism involving extracellular zinc release and activation of neuronal NADPH oxidase.

Introduction

Insulin and sulfonylurea therapy for diabetes mellitus carries the risk of hypoglycemic brain injury, and this risk is a major impediment to optimal glucose regulation in diabetic patients (1, 2). Depending upon its severity, hypoglycemia (HG) can cause irritability, impaired concentration, focal neurological deficits, seizures, coma, and, with profound HG, neuronal death (3–5). Hypoglycemic neuronal death is most pronounced in specific neuron populations: neurons in the hippocampal CA1, subiculum, and dentate granule cell layer; cortical layers 2 and 3 of cerebral cortex; and the dorsolateral striatum (6, 7). The hippocampal neurons in particular are important for learning and memory, and patients who survive hypoglycemic coma may be left with significant cognitive impairment (8, 9).

The neuronal death resulting from HG is not a straightforward result of energy failure but instead results from a sequence of events initiated by HG. These events include activation of neuronal glutamate receptors (10–12), production of ROS (13, 14), neuronal zinc release (15), activation of poly(ADP-ribose) polymerase–1 (16, 17), and mitochondrial permeability transition (18, 19). Importantly, correction of plasma glucose concentration alone does not interrupt this cell death process (16, 17).

Several studies point to oxidative DNA damage as a critical event in this sequence of events (12, 14, 16, 18), but the source and mechanism of oxidant production have not been established. Mitochondria have been implicated as a source of ROS in many disorders, including ischemia-reperfusion (20), and mitochondria taken from brain during HG exhibit increased capacity to generate ROS (21); however, ROS can be generated by several sources other than mitochondria. Among these sources is NADPH oxidase, a superoxide-generating enzyme long recognized as crucial for the bactericidal function of neutrophils (22). Recent studies have identified NADPH oxidase also in neurons (23–25), where it may normally function in physiological redox signaling (26). Activation of NADPH oxidase in neutrophils can kill neighboring cells (22), and activation of NADPH oxidase in neurons can similarly contribute to cell death under some conditions (27).

In this study we used cell culture and rodent models of HG to identify the source and mechanism of neuronal superoxide production. Surprisingly, superoxide production was found to occur mainly during the period of glucose reperfusion (GR), rather than during HG itself. Our results also indicate that neuronal NADPH oxidase is the primary source of neuronal oxidative stress after HG and that the rate of superoxide production is influenced by the blood glucose concentration achieved in the immediate posthypoglycemic period.

Results

Superoxide is produced at the time of GR after HG. To characterize the source of superoxide production in hypoglycemic neuronal injury, we used a rat model of insulin-induced HG and evaluated the production of ROS with dihydroethidium (28). Dihydroethidium is oxidized by superoxide and superoxide reaction products to form fluorescent ethidium (Et) species (29), which are then trapped within cells by DNA binding. Rats subjected to 60 minutes of profound HG (producing an isoelectric EEG) showed only a modest increase in neuronal Et fluorescence, but rats undergoing only 30 minutes of HG followed by a subsequent 30-minute interval of GR showed a several-fold increase in neuronal Et fluorescence

Nonstandard abbreviations used: CaEDTA, calcium disodium EDTA; Et, ethidium; GD, glucose deprivation; GFAP, glial fibrillary acidic protein; GR, glucose reperfusion; HG, hypoglycemia; MAP2, microtubule-associated protein–2; SOD, superoxide dismutase; tempol, 4-hydroxy-2,2,6,6-tetramethylpiperidinyloxy; TSQ, (6 methoxy 8 quinolyl) para toluenesulfonamide; ZnEDTA, zinc EDTA.

Conflict of interest: The authors have declared that no conflict of interest exists.

Citation for this article: *J. Clin. Invest.* **117**:910–918 (2007). doi:10.1172/JCI30077.

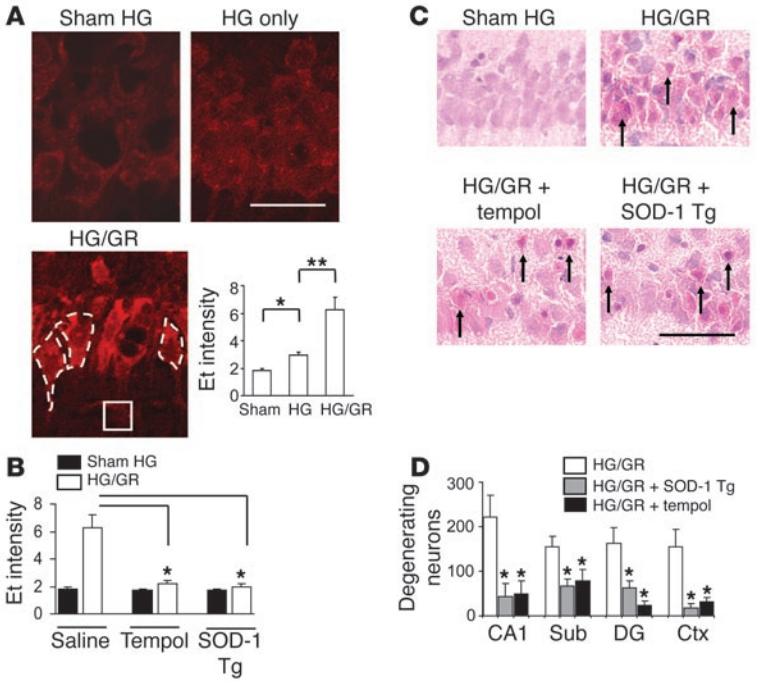

Figure 1
GR induces neuronal superoxide production after HG. (**A**) Neuronal superoxide production as imaged by Et fluorescence in rat brain hippocampal sections after sham HG (Sham), 60 minutes of HG without GR (HG only), or 30 minutes of HG plus 30 minutes of GR (HG/GR). Et signal intensity is expressed as the ratio of the mean fluorescence in neuronal perikarya (example outlined in white dashed line) to background (stratum radiatum; white square). Scale bar: 100 μm. Data are mean + SEM; $n = 4$; $^*P < 0.05$; $^{**}P < 0.01$. (**B**) Et fluorescence induced by HG/GR was blocked by tempol and by overexpression of SOD-1 (SOD-1 Tg). Data are mean + SEM; $n = 3$–5; $^*P < 0.05$. (**C**) Tempol and SOD-1 overexpression also reduced neuronal death after HG/GR. H&E-stained sections of the hippocampal CA1 cell layer prepared 7 days after HG/GR show degenerating neurons with pyknotic, eosinophilic changes (arrows). Scale bar: 100 μm. (**D**) The number of degenerating neurons was quantified in 4 brain regions: hippocampal CA1, subiculum (Sub), dentate gyrus (DG), and perirhinal cortex (Ctx). Data are mean + SEM; $n = 7$–10; $^*P < 0.05$ versus HG/GR alone in each region.

despite the shorter hypoglycemic interval (Figure 1A), suggesting that ROS are produced primarily during GR. The Et formation induced by HG/GR was blocked by the superoxide dismutase (SOD) mimic tempol (4-hydroxy-2,2,6,6-tetramethylpiperidinyloxy) (50 mg/kg) and was also blocked in transgenic rats that overexpress SOD-1 (30), confirming that the Et fluorescence signal results primarily from the production of superoxide (Figure 1B). Tempol and SOD-1 overexpression also reduced neuronal death (Figure 1, C and D), thus linking superoxide production to HG-induced neuronal death. Blood glucose concentrations were not significantly different among the 3 treatment groups (Table 1).

Superoxide is produced primarily by NADPH oxidase. To identify the site and mechanism of HG-induced superoxide production, we subjected cortical cell cultures, containing neurons and glia, to glucose deprivation (GD) followed by GR. As observed with HG in vivo, GD alone caused only a negligible increase in the Et signal, but GR produced a rapid increase in neuronal Et fluorescence (Figure 2A). Control cultures, in which 10 mM glucose was added back after less than 5 minutes of GD, exhibited a negligible Et signal (Figure 2B). GR with 2 mM glucose produced a slightly smaller signal than GR with 10 mM glucose (Figure 2B), and all subsequent studies were performed using 10 mM glucose replacement. Detection of the lipid peroxidation product 4-hydroxynonenal in neurons after GD/GR, but not GD alone, provided additional evidence that GR triggers superoxide formation (Figure 2C).

Mitochondria have been identified as a source of neuronal superoxide production in glutamate excitotoxicity (31), and glutamate excitotoxicity contributes to hypoglycemic neuronal death (7, 10, 12). We therefore evaluated superoxide production in the presence of the complex I inhibitor rotenone (5 μM), the complex II inhibitor 2-thenoyltrifluoroacetone (10 μM), and the mitochondrial uncoupler carbonyl cyanide 4-(trifluoromethoxy)phenylhydrazone (0.5 μM), each of which prevents superoxide production by the mitochondrial electron transport chain (32). None of these agents prevented neuronal superoxide production during GD/GR (Figure 2D). Superoxide can also be generated from dehydrogenase complexes of the mitochondrial tricarboxylic acid cycle (33); however, neuronal superoxide production after GD/GR was similarly unaffected by inhibiting glucose-derived substrate delivery to mitochondria with either 500 μM iodoacetate to inhibit glycolysis or with 250 μM α-cyano-4-hydroxycinnamate (OHCA) to block mitochondrial pyruvate uptake (Figure 2, C and D).

A third potential source of superoxide generation is NADPH oxidase, which requires glucose for regeneration of NADPH by the hexose monophosphate shunt (22). Incubation with either 500 μM 6-aminonicotinamide, an inhibitor of the hexose monophosphate

Table 1
Blood glucose concentration during HG and GR

Treatment group	Arterial glucose concentration (mM)			
	Fasting (before insulin)	HG (isoelectric EEG)	30 min after GR	60 min after GR
5–10 mM	4.34 ± 0.15 ($n = 7$)	0.40 ± 0.02	8.02 ± 0.46	7.53 ± 0.39
5–10 mM + tempol	4.28 ± 0.35 ($n = 5$)	0.38 ± 0.06	7.70 ± 0.43	7.37 ± 0.51
5–10 mM SOD-1 Tg	4.42 ± 0.21 ($n = 7$)	0.37 ± 0.05	7.49 ± 0.44	7.14 ± 0.48
10–15 mM	4.48 ± 0.32 ($n = 4$)	0.33 ± 0.07	14.50 ± 1.49[A]	14.03 ± 1.29[A]
1–2 mM	4.25 ± 0.19 ($n = 7$)	0.38 ± 0.02	1.64 ± 0.11[B]	1.71 ± 0.11[B]

Data represent arterial glucose concentrations (mM) in each of the 3 target GR ranges, in WT rats with and without tempol treatment, and in SOD-1 Tg rats. Data are mean ± SEM. [A]$P < 0.05$ versus the GR 5–10 mM group; [B]$P < 0.01$ versus the GR 5–10 mM group.

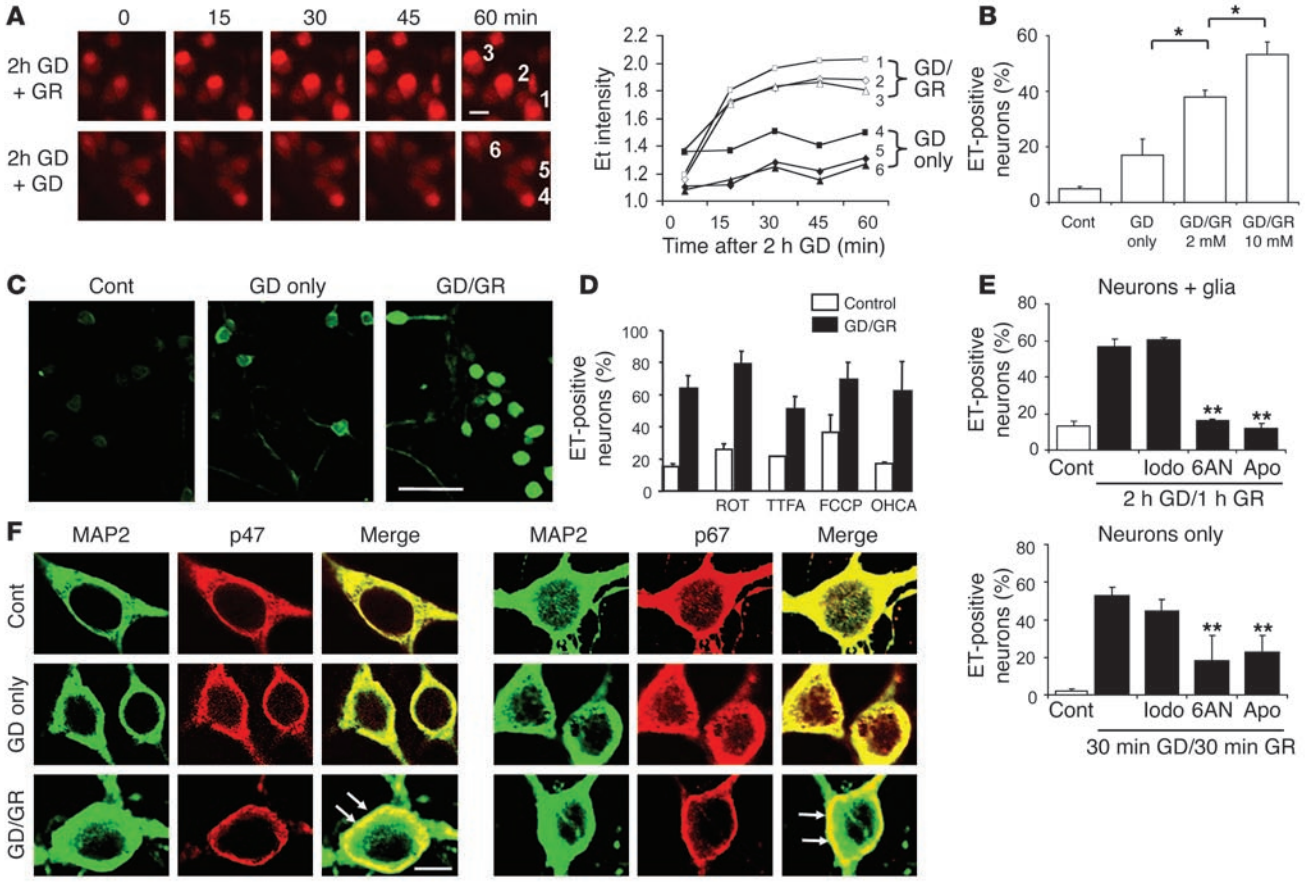

Figure 2

Neuronal superoxide production after GD/GR is due to NADPH oxidase activation. (**A**) Et fluorescence in cultured mouse neurons at time points after GD and GR. Top row shows neurons subjected to 2 hours of GD followed by GR; bottom row shows neurons subjected to GD during the entire 3-hour interval. Line graphs show the change in Et fluorescence over time in each of the labeled neurons, with values normalized to the background signal. Scale bar: 30 μm. (**B**) Quantification of Et-positive neurons in cultures treated with 3 hours GD alone or with 2 hours GD followed by 1 hour GR at the designated glucose concentration. Controls (Cont) received 10 mM glucose after less than 5 minutes of GD. Data are mean + SEM; $n = 7$; $^*P < 0.01$. (**C**) Immunostaining for 4-hydroxynonenal in cultured neurons. Representative of $n = 3$. Scale bar: 100 μm. (**D**) Neuronal superoxide production induced by GD/GR was not blocked by inhibitors of mitochondrial superoxide production. ROT, rotenone; TTFA, 2-thenoyltrifluoroacetone; FCCP, carbonyl cyanide 4-(trifluoromethoxy)phenylhydrazone; OHCA, α-cyano-4-hydroxycinnamate. $n = 4$. (**E**) Superoxide production was also unaffected by the glycolytic inhibitor iodoacetate (Iodo) but was blocked by 6-aminonicotinamide (6AN) and by apocynin (Apo). This pattern was also observed in neurons cultured in the absence of glia (bottom panel). Data are mean + SEM; $n = 4$; $^{**}P < 0.05$. (**F**) Immunostaining for the $p47^{phox}$ (left panels) or $p67^{phox}$ (right panels) subunits of NADPH oxidase showed their migration to the neuronal plasma membrane (arrows) after GD/GR but not after GD alone. MAP2 immunostaining demarcates the neuronal cytoplasmic space. Scale bar: 10 μm.

shunt (34), or with 500 μM apocynin (4-hydroxy-3-methoxyacetophenone), an inhibitor of NADPH oxidase activity (35), blocked the superoxide production induced by GD/GR in cortical cell cultures (Figure 2E). Since cortical cultures contain astrocytes and microglia in addition to neurons, these studies were also performed in cultures containing neurons alone to determine which cell type was the source of superoxide production. Cultures containing neurons in the absence of glia produced the same pattern of results obtained with the neuron/glia cocultures, although a shorter interval of GD was required to induce comparable superoxide production (Figure 2E).

NADPH oxidase is composed of several subunits, including the $p47^{phox}$ and $p67^{phox}$ subunits, which coalesce at the plasma membrane to form the active enzyme complex (22, 36). Immunostaining confirmed the presence of these subunits in neurons and showed their translocation to the neuronal plasma membrane after GD/GR but not after GD alone (Figure 2F).

Inhibition of NADPH oxidase prevents superoxide production and subsequent neuronal death. To confirm further that NADPH oxidase is the source of superoxide production after GD/GR, we prepared cortical cocultures consisting of neurons from WT mice or from $p47^{phox}$-deficient mice, with the neurons plated onto WT glia. Cells from $p47^{phox}$-deficient mice are unable to assemble an active NADPH oxidase complex (37, 38). The $p47^{phox}$-deficient neurons generated much less superoxide after GD/GR and showed less neuronal death than WT neurons (Figure 3A). This effect was comparable to that obtained in WT neurons treated with 500 μM apocynin or 500 μM 6-aminonicotinamide (Figure 3B). We then used the $p47^{phox}$-deficient mice to evaluate superoxide production and neuronal survival after HG in vivo. Mice lacking $p47^{phox}$ showed much less neuronal death than WT mice of the same C57/B6 background strain (Figure 3C), and this reduction in cell death was accompanied by reduced neuronal Et fluorescence at

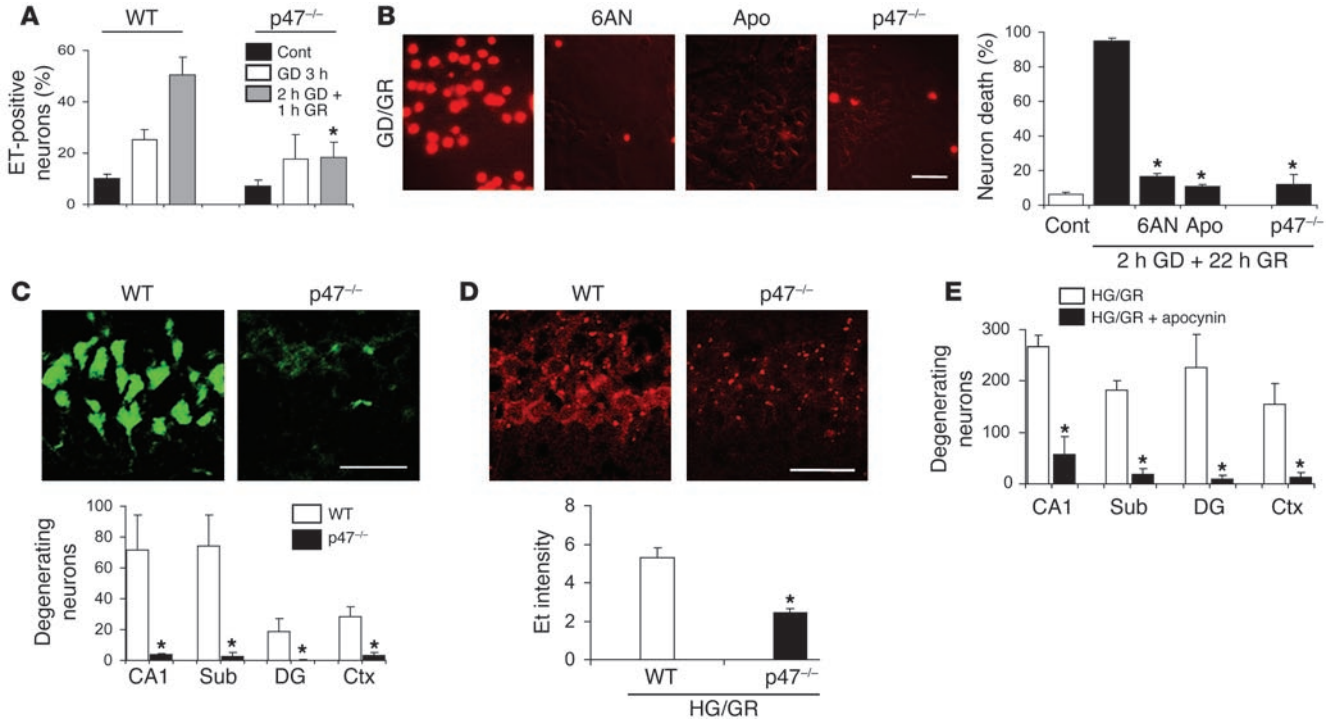

Figure 3

Inhibition of NADPH oxidase prevents HG-induced neuronal death. (**A**) GD/GR-induced superoxide production in cortical neurons is attenuated by p47^{phox} deficiency. Data are mean + SEM; $n = 3$; $^*P < 0.05$ versus WT. (**B**) GD/GR-induced neuronal death is blocked by p47^{phox} gene deletion and by pharmacological inhibitors of NADPH oxidase activity. Photomicrographs show propidium iodide (PI) staining of dead neurons 22 hours after GD in WT neurons, p47^{phox}-deficient neurons, or WT neurons treated with 6-aminonicotinamide or apocynin. Scale bar: 100 μm. Data are mean + SEM; $n = 4$–6; $^*P < 0.05$. (**C**) Photomicrographs show dead neurons stained green by Fluoro-Jade B in the hippocampal CA1 region of WT and p47^{phox}-deficient mice 7 days after HG/GR. Graph quantifies hypoglycemic neuronal death in 4 vulnerable brain regions. Scale bar: 100 μm; data are mean + SEM; $n = 3$; $^*P < 0.05$. (**D**) HG/GR-induced superoxide production, as evidence by Et fluorescence, was attenuated in neurons of p47^{phox}-deficient mice. Scale bar: 100 μm; data are mean + SEM; $n = 3$–4; $^*P < 0.05$. (**E**) Apocynin reduced neuronal death in WT rats evaluated 7 days after HG/GR. Data are mean + SEM; $n = 5$; $^*P < 0.05$.

the time of reperfusion (Figure 3D). A comparable reduction in cell death was observed in WT rats treated with 15 mg/kg apocynin to inhibit NADPH oxidase previous to GR (Figure 3E).

Zinc chelation prevents superoxide production during GR. The mechanism by which NADPH oxidase is activated in nonphagocytic cells such as neurons is not well understood, but zinc has been identified as both an inducer of neuronal NADPH oxidase activity (39) and a contributor to hypoglycemic neuronal death (15). We examined intracellular free zinc concentrations in cultured neurons using the fluorescent dye FluoZin-3 (40). FluoZin-3 fluorescence intensity was increased by 52% ± 11% in neurons subjected to 3 hours of GD and by 203% ± 19% in neurons treated with only 2 hours of GD followed by 1 hour of glucose replacement ($n = 4$; $P < 0.01$). Cultures treated with 50 μM of the extracellular zinc chelator calcium disodium EDTA (CaEDTA) (41) showed a significantly reduced FluoZin-3 signal after GD/GR (Figure 4A). Specificity of the FluoZin-3 signal was confirmed by near-complete suppression of the fluorescent signal by 100 μM of the cell-permeant heavy metal chelator TPEN [N,N,N′,N′-tetrakis(2-pyridyl-methyl)ethylenediamine] (40). The translocation of p47^{phox} and p61^{phox} to the neuronal cell membrane in cortical cultures treated with GD/GR was similarly blocked by CaEDTA but not zinc EDTA (ZnEDTA), which lacks zinc chelating capacity (Figure 4B).

Extracellular zinc in brain is derived primarily from release of synaptic vesicles (42). We used the fluorescent dye TSQ [(6 methoxy 8 quinolyl) para toluenesulfonamide], which binds chelatable zinc (43), to determine whether vesicular zinc release is associated with NADPH oxidase activation after induction HG and GR (Figure 4C). Vesicular zinc in the hippocampal hilus region stains brightly with TSQ under basal conditions. The vesicular zinc signal was partially depleted by 60 minutes of HG alone but was almost completely depleted by 30 minutes of HG followed by 30 minutes of GR. Conversely, TSQ staining for zinc in the postsynaptic pyramidal cell bodies was absent under control conditions or HG alone but increased after HG/GR (Figure 4D), suggesting that zinc released from synaptic vesicles is translocated into the postsynaptic cells under these conditions. This increase was blocked in rats given intracerebroventricular injection of the zinc chelator CaEDTA. Rats treated with CaEDTA also showed reduced neuronal superoxide formation, suggesting that vesicular zinc release is upstream of NADPH oxidase activation. ZnEDTA, used as a control, had no effect (Figure 4E).

Post-HG glucose concentrations influence neuronal superoxide production. Results of the cell culture studies presented here are consistent with prior reports that glucose flux through the hexose monophosphate shunt is required for regeneration of the NADPH substrate used by NADPH oxidase (34, 44). A previous

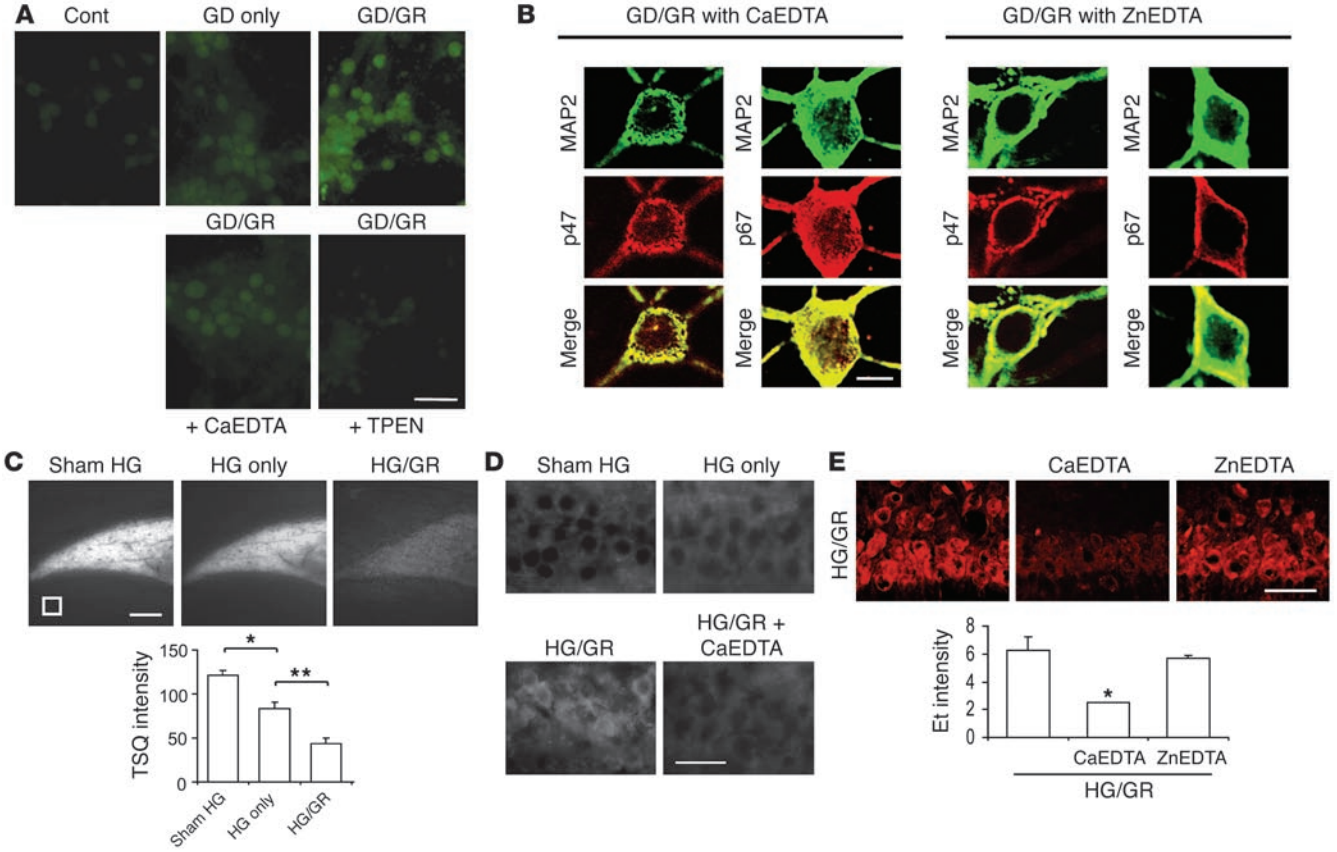

Figure 4
Zinc chelation prevents activation of neuronal NADPH oxidase. (**A**) FluoZin-3 images of intracellular free zinc levels in cultured neurons after 3 hours of GD or 2 hours of GD and 1 hour of glucose replacement (GD/GR). Fluorescence induced by GR was attenuated in cultures treated with CaEDTA during the GD/GR incubations and eliminated by 10-minute incubation with N,N,N',N'-tetrakis(2-pyridyl-methyl)ethylenediamine (TPEN). $n = 4$. (**B**) Immunostaining for the $p47^{phox}$ and $p67^{phox}$ subunits of NADPH oxidase in cultured neurons. GD/GR-induced migration of these subunits to the neuronal plasma membrane was blocked by the zinc chelator CaEDTA but not by ZnEDTA used as a control. Scale bar: 10 μm. Representative of 3 cultures under each condition. (**C**) Vesicular zinc in the rat hippocampal hilus is imaged with TSQ fluorescence (white). The TSQ signal loss was greater after 30 minutes HG and 30 minutes GR (HG/GR) than after 60 minutes HG without GR. Fluorescence intensity is expressed as arbitrary units, with subtraction of background measured in the lateral ventricle (white square). Scale bar: 200 μm. Data are mean + SEM; $n = 10$; $^*P < 0.05$; $^{**}P < 0.01$. (**D**) TSQ fluorescence was increased in the postsynaptic pyramidal cells after HG/GR, and this increase was blocked by CaEDTA ($n = 3$). Scale bar: 100 μm. (**E**) CaEDTA reduces GR-induced superoxide production in the CA1 neurons. ZnEDTA was the control. Graph shows quantified CA1 neuronal Et fluorescence intensity in rats treated with intracerebroventricular saline, CaEDTA, or ZnEDTA. Scale bar: 100 μm. Data are mean + SEM; $n = 3$–5; $^*P < 0.05$.

study also suggested that high blood glucose concentrations following HG can exacerbate brain injury (45). We therefore assessed the effects of differing blood glucose concentrations during the immediate reperfusion period on neuronal superoxide production and survival. Rats were given glucose at rates that maintained blood glucose concentration in the range of 1–2 mM, 5–10 mM, or 10–15 mM following HG (Table 1). Anesthesia was discontinued after 2 hours, at which time the rats were allowed to feed ad libitum. Rats in the 1–2 mM glucose group exhibited reduced neuronal death (evaluated at 7 days) relative to the 5–10 mM group (Figure 5A). Rats in the 1–2 mM glucose group also showed reduced neuronal superoxide production during GR (Figure 5B). Rats in the 10–15 mM glucose group did not exhibit any further increase in neuron death relative to the 5–10 mM group. There was negligible Et signal in the "sham HG" rats given glucose (in addition to insulin) to maintain blood glucose in the 5–10 mM range.

Discussion

These studies present what we believe to be 3 novel findings: hypoglycemic neuronal death is triggered by GR rather than by HG per se; the primary source of superoxide generation in HG-reperfusion is neuronal NADPH oxidase, rather than mitochondria; and HG-induced activation of neuronal NADPH oxidase involves zinc as a signaling molecule.

HG of varying severity is common in diabetic patients, particularly among those attempting tight glucose control (1, 2). The degree of HG modeled in the present studies is extreme, corresponding to the clinical setting of deep hypoglycemic coma in which blood glucose concentrations often fall below 1 mM (5, 8, 46) and brain glucose concentrations fall to near zero (47). Patients in hypoglycemic coma are treated with concentrated glucose solutions, which typically elevate blood glucose to supranormal values (2, 46, 48). The cell culture and in vivo models of HG employed here approximate this setting of pro-

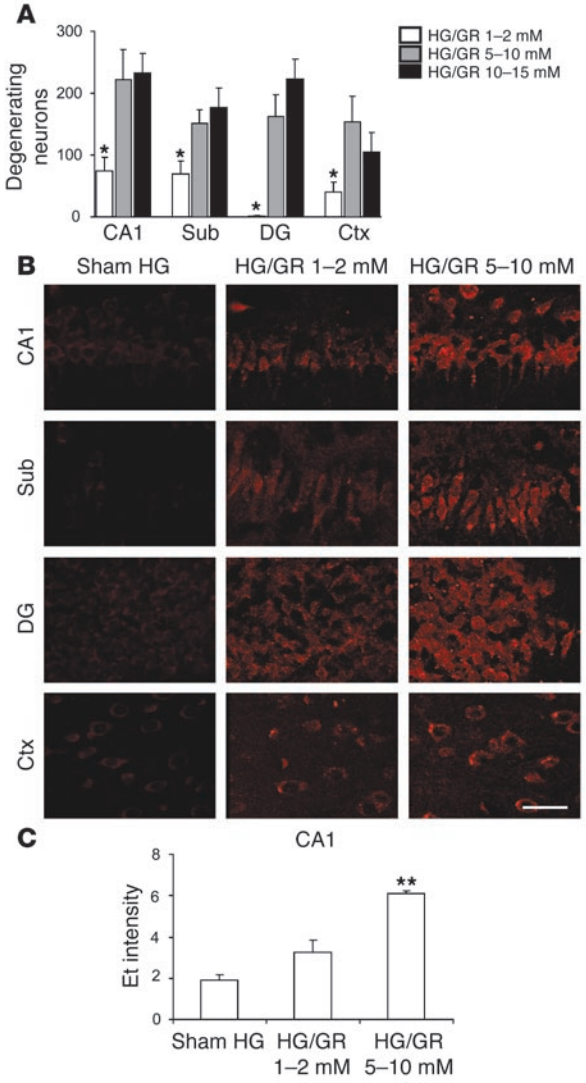

Figure 5
Effects of reperfusion glucose concentrations on neuronal superoxide production and survival. (**A**) Effects of reperfusion blood glucose concentrations on neuronal survival after HG/GR. Data are mean + SEM; $n = 7–10$; $^{*}P < 0.01$ versus the 5–10 mM GR group in each region. (**B**) Neuronal superoxide production as imaged by Et fluorescence in rat brain hippocampal sections after HG and GR at the indicated blood glucose concentrations. Sham HG rats received glucose infusions immediately after insulin to prevent HG. Scale bar: 100 μm. (**C**) Et signal intensity was quantified for the CA1 region as described for Figure 1A. Data are mean + SEM; $n = 4$; $^{**}P < 0.05$.

found HG and glucose correction, in which brain injury can be a disabling or lethal sequela (2, 8, 46).

The finding that superoxide production occurs predominately after GR, in both the cell culture and in vivo HG studies, corroborates prior observations on the sequence of events leading to hypoglycemic neuronal death. In a rat model of insulin-induced HG, the formation of nitrotyrosine was detected shortly after GR, not during the HG interval (16). Similarly, activation of poly(ADP-ribose) polymerase-1 (PARP-1), an enzyme responsive to DNA damage, was detected only after GR (16). HG/GR thus has similarities to ischemia-reperfusion, in which oxidative stress is attributed to reintroduction of oxygen to damaged tissue (49). A fundamental difference, however, is that brain oxygen tension is essentially unchanged during HG and GR, and thus reintroduction of glucose, not oxygen, is responsible for the oxidant production in this setting. The present findings suggest that the reintroduction of glucose might also be a key factor in reperfusion injury after ischemia.

A modest increase in ROS production was observed during GD, in addition to the much larger increase induced by GR, in both the cell culture and the in vivo studies. The source of ROS produced during HG was not evaluated in the present studies, but a prior report suggests that brain mitochondria isolated during HG (without GR) produce more ROS than control mitochondria (21). However, the present results suggest that NADPH oxidase, rather than mitochondria, are the primary source of superoxide production during the GR period.

NADPH oxidase is a multicomponent enzyme comprising a plasma membrane–bound subunit, gp91; a membrane-associated flavocytochrome, cytochrome b558; and at least 3 cytosolic subunits, $p47^{phox}$, $p67^{phox}$, and the small G protein Rac2 (36). During activation, the $p47^{phox}$ component is phosphorylated and migrates to the plasma membrane, where it associates with the other subunits to form the active enzyme complex. The methoxy-substituted catechol apocynin blocks this assembly but does not inhibit mitochondrial dehydrogenases (50, 51). In the present studies, apocynin blocked the production of superoxide induced by GR in both the cell culture and in vivo preparations. In addition, mice deficient in the $p47^{phox}$ subunit of NADPH oxidase exhibited reduced superoxide production and reduced neuronal death after HG/GR. The coculture studies using $p47^{phox}$-deficient neurons with WT glia showed in addition that activation of NADPH oxidase in neurons alone can be sufficient to cause neuronal death, although these results do not exclude a neurotoxic role for microglial or astrocyte NADPH oxidase in vivo.

A third, more indirect line of evidence supporting NADPH oxidase as the primary source of superoxide production also links NADPH oxidase activity to GR. Ongoing production of NADPH is required for NADPH oxidase activity in nonneuronal cell types (34, 44). NADPH is regenerated through the hexose monophosphate shunt, which requires glucose as a substrate. In the present studies, inhibition of the hexose monophosphate shunt with 6-aminonicotinamide blocked both neuronal superoxide production and neuronal death, a result that is not readily explained by any mechanism other than reduced NADPH oxidase activity.

Zinc can activate NADPH oxidase in neurons through a signaling pathway involving protein kinase C (27, 39). This is germane to hypoglycemic neuronal injury because several neuronal populations release zinc in response to depolarizing stimuli (52); each of the brain regions most vulnerable to HG contain high concentrations of presynaptic vesicular zinc (42); and intracerebroventricular administration of a zinc chelator (CaEDTA) can prevent hypoglycemic neuronal death (15). The present studies suggest that zinc effects on hypoglycemic neuronal death are attributable to its activation of NADPH oxidase. Intracellular zinc levels increased during GR, and preventing this increase with CaEDTA blocked assembly of the NADPH oxidase complex, superoxide production, and neuronal death. Since CaEDTA is an extracellular zinc chelator, this suggests that the zinc elevations result from an influx of extracellular zinc derived either from vesicular zinc release or, in

cultured cells, from ambient zinc in the culture medium. However, we cannot entirely exclude the alternative possibility that CaEDTA lowers intracellular zinc stores during the incubation period (53).

The relationship between glutamate excitotoxicity and NADPH oxidase is not clearly resolved by the present studies. HG causes several-fold elevations in brain extracellular glutamate concentrations, and pretreatment with glutamate receptor antagonists prevent hypoglycemic neuronal death (10–12). Although glutamate excitotoxicity induces superoxide production, this is thought to arise primarily from the mitochondria (31) rather than NADPH oxidase. The timing of glutamate release relative to the other events in this process is also uncertain. Here we found that vesicular zinc release from presynaptic mossy fibers occurs primarily during the period of GR. Since glutamate and zinc are colocalized in excitatory synaptic terminal vesicles (52, 54), it is possible that glutamate release from synaptic terminals also occurs at the time of GR. Further studies will be required to settle these issues.

The present studies show that hypoglycemic neuronal death is triggered by GR; however, the clinical treatment of HG requires correction of blood glucose levels. Thus, the finding that superoxide formation and neuronal survival are influenced by the rate of blood glucose elevation after HG may have implications for the management of hypoglycemic coma. Restoring blood glucose to 1–2 mM during the first hour after HG resulted in less superoxide production and less neuronal death than restoration to higher glucose levels (>5 mM). These data suggest that a gradual correction of blood glucose in patients with hypoglycemic coma may be preferable to more rapid correction and hyperglycemia. We emphasize, however, that the specific blood glucose values obtained in the rodent studies cannot be directly applied to human patient care settings and that the results of these studies may not apply to less severe HG.

The biochemical mechanism of this effect was not established here, but one possibility is that glucose transport across the blood-brain barrier is accelerated at higher glucose concentrations (47), thereby increasing glucose entry into the hexose monophosphate shunt. This would facilitate the regeneration of NADPH and thus facilitate NADPH oxidase activity (34, 44). The much smaller deleterious effect of high glucose concentrations after GD in the cell culture studies (Figure 2B) is consistent with an effect at the blood-brain barrier.

Methods

The studies were approved by the San Francisco Veterans Affairs Medical Center animal studies committee. Rats (Sprague-Dawley) were obtained from Charles River Laboratories. Rats in the SOD-1 Tg colony were maintained as heterozygotes, with outbreeding to WT rats. Experiments with the SOD-1 Tg rats used the non-Tg littermates as controls. The $p47^{phox}$-deficient mice and the WT mice used as their controls were of the C57/B6 strain, both obtained from The Jackson Laboratory. All other mice were of the CD-1 strain (Simonsen Laboratories). Cell culture reagents were obtained from Mediatech Inc. All other reagents were obtained from Sigma-Aldrich except where noted.

Cell cultures. Mouse cortical cultures were prepared by plating embryonic neurons onto a preexisting glia layer at a density of 6×10^5 cells/cm^2 and used at neuronal age 20–22 days in vitro (55). Glia-free neuron cultures were prepared by plating the embryonic neurons directly onto a plastic surface or, for immunostaining, onto poly-D-lysine–coated glass coverslips (56). These cells were cultured in glia-conditioned medium and used at days 10–14 in vitro, at which time the cultures contained greater than 95% neurons, as assessed by immunostaining for the neuron marker microtubule-associated protein–2 (MAP2) and the astrocyte marker glial fibrillary acidic protein (GFAP) (56). Glucose concentration in the culture media was 4.0–5.5 mM.

GD in cell cultures. The culture medium was exchanged with a bicarbonate-buffered balanced salt solution (BSS) containing (in mM) KCl, 3.1; NaCl, 134; $CaCl_2$, 1.2; $MgSO_4$, 1.2; KH_2PO_4, 0.25; $NaHCO_3$, 15.7; glucose, 0. The pH was adjusted to 7.2 while the solution was equilibrated with 5% CO_2 at 37°C. Osmolarity was verified at 290–310 mOsm with a Wescor vapor pressure osmometer. Drugs were added from concentrated stocks prepared in BSS immediately before use and adjusted to pH 7.2 when necessary. After a 5-minute period to allow complete egress of glucose from the cells, the culture medium was completely exchanged a second time, and the cultures were placed in a 37°C, 5% CO_2 incubator. GD was terminated at the designated time points by adding 2 or 10 mM glucose back to the medium. Control wells received 10 mM glucose replacement immediately after the initial medium exchange.

Immunostaining. Immunostaining was performed as described previously (56). Astrocytes and neurons were identified by immunoreactivity to GFAP and MAP2, respectively. Cell cultures were fixed with 1:1 methanol/acetone at 4°C for 10 minutes, then incubated for 30 minutes in blocking buffer (0.01% PBS/2% goat serum/0.2% Triton-X/0.1% BSA). Cultures were incubated with rabbit anti-MAP2 or rabbit anti-GFAP (Chemicon), diluted 1:1,000 in blocking buffer, then incubated with anti-rabbit IgG conjugated with Texas red or Alexa Fluor 594 (Molecular Probes; Invitrogen) diluted 1:300 in blocking buffer. 4-Hydroxy-2-nonenal formation was identified by immunostaining with a 1:500 dilution of mouse monoclonal antibody against 4-hydroxy-2-nonenal (Alpha Diagnostic International). Primary antibody binding was visualized with a 1:250 dilution of Alexa Fluor 488–conjugated anti-mouse IgG (Molecular Probes; Invitrogen). Subcellular localization of the $p47^{phox}$ or $p67^{phox}$ subunits of NADPH oxidase was evaluated in cultures fixed with 4% paraformaldehyde for 20 minutes on ice. The cultures were dehydrated in ethanol washes and air dried. After preincubation in blocking buffer, the cultures were incubated with either a 1:500 dilution of mouse anti-$p47^{phox}$ or a 1:500 dilution of mouse anti-$p67^{phox}$ (BD Biosciences — Transduction Laboratories), together with a 1:200 dilution of rabbit monoclonal anti-MAP2 antibody (BD Biosciences — Transduction Laboratories). After washing, the cultures were incubated with 1:250 dilutions of Alexa Fluor 488– and 594–conjugated goat anti-rabbit IgG (Molecular Probes; Invitrogen). Negative controls were prepared by omitting the primary antibodies.

HG in vivo. Insulin-induced HG in rats was induced as described previously, with the period of severe HG defined here as the interval during which the EEG exhibited an isoelectric pattern (16, 57). Rats (250–350 g) were fasted overnight. Anesthesia was induced with 3% isoflurane in a 75:25 mixture of nitrous oxide and oxygen (Air Liquide America). After intubation, rats were ventilated with a small-animal respirator (Harvard Apparatus), and isoflurane content was reduced to 1%. A femoral artery line was placed for blood sampling and for blood pressure monitoring. Blood gases were measured at 1-hour intervals using an I-STAT machine (Abbott). Tidal volume and oxygen flow were adjusted to keep $PaCO_2$ between 35 and 45 mmHg and PaO_2 above 100 mmHg. Blood pressure and EEG were continuously monitored and recorded (BIOPAC Systems Inc.). Core temperature was kept at 36.5–37.5°C with a heating blanket. HG was induced by intraperitoneal injection of 10 U/kg of regular insulin (Novolin-R; Novo Nordisk). Blood glucose was measured at serial time points in rat with a YSI 2700 glucose analyzer (YSI Life Sciences). Mean arterial blood pressure was maintained between 160 and 200 mmHg during the entire EEG isoelectric period by adjusting the isoflurane concentration, and bradycardia was prevented with intramuscular injection of atropine (1 mg/kg). EEG was monitored using needle electrodes placed

in the cortical surface. Burr holes were made in the skull bilaterally over parietal cortex, and monopolar electrodes were inserted beneath the dura. A reference needle was placed in neck muscle. HG was terminated in most studies by injection of 0.2 ml of 50% glucose via the femoral vein, followed by continuous infusion of 1:1 solution of 50% glucose and Krebs-Henseleit buffer (1.5 ml/hour for 3 hours) and supplemented by 1 ml of 25% glucose by intraperitoneal injection at 1 hour after the start of the intravenous glucose infusions. In studies examining reduced glucose infusion rates, HG was terminated by 25% glucose in Krebs-Henseleit buffer (0.75 ml/h for 3 hours) without any bolus injection. For the high GR group, HG was terminated by infusion of 50% glucose in Krebs-Henseleit buffer (1.5 ml/h for 3 hours) along with a bolus injection of 0.2 ml of 50% glucose through the femoral vein. Sham HG controls were prepared by intravenous administration of 1.5 ml/h of 25% glucose simultaneously with 10 U/kg of insulin to maintain a plasma glucose level between 5 and 10 mM for 5 hours. Where used, tempol (50 mg/kg) was injected by femoral vein, and apocynin (15 mg/kg) was injected intraperitoneally, immediately before the start of GR. The drugs were dissolved in 1% DMSO vehicle, and control rats for these studies received equal volumes of vehicle alone. In some studies, rats were euthanized immediately after HG without GR. In all other studies, the rats were returned to their cages once they were awake and ambulatory.

For studies in mice, the insulin dose was reduced to 5 U/kg and the isoelectric period was extended to 45 minutes before glucose reinfusion or tissue harvest. Anesthesia, temperature regulation, and EEG recording were performed as described for rat HG, with the exception that hexamethonium chloride was administered at 30 mg/kg intraperitoneally 15 minutes before the insulin administration to reduce autonomic responses (58). In a separate cohort of mice, mean arterial pressure was monitored with a femoral artery cannula. Mice treated with hexamethonium did not exhibit mean arterial blood pressure values below 75 mmHg (data not shown). Serial 10-μl blood samples for glucose measurements were obtained from the tail artery. Mouse HG was terminated by a bolus injection of 25% glucose (100 μl) into intraperitoneal space, and the subsequent blood glucose level was maintained between 5 and 10 mM by subcutaneous injection of 25% glucose (100 μl/30 minutes) until animals were ambulatory.

Intracerebral injections. As described previously (59), a burr hole was made 1.0 mm caudal to bregma, 1.5 mm lateral to the midline, and the syringe needle tip was lowered 3.0 mm below the dura. CaEDTA and ZnEDTA were prepared as 100-mM solutions in physiological saline and brought to neutral pH with NaOH. Five microliters of saline, 100 mM CaEDTA in saline, or 100 mM of ZnEDTA in saline was injected into the right lateral ventricle over a 5-minute period. The injections were begun immediately following the 30 minute EEG isoelectric intervals.

Superoxide detection. For the studies in brain, dihydroethidium (Molecular Probes; Invitrogen) was prepared as a 1 mg/ml solution in 1% DMSO and administered at 1 mg/kg by femoral vein at the onset of EEG isoelectricity. Animals were euthanized at the indicated time points and perfusion fixed with 4% paraformaldehyde. Twenty-micrometer cryostat sections were prepared and photographed with a confocal fluorescence microscope with excitation at 510–550 nm and emission greater than 580 nm to detect Et (30). Five sections were analyzed from each brain, taken at 80-μm intervals to span the hippocampus. Et signal intensity was expressed as the ratio of the mean fluorescence in neuronal perikarya to fluorescence in the stratum radiatum of the hippocampal CA1 region. For cell culture studies, 1 μM dihydroethidium (60) was added to the cultures at the beginning of GD. The cultures were photographed with a fluorescence microscope at the designated time points, and the digitized images were analyzed and expressed as percentage of neurons with an Et signal at least 50% higher than background. In some studies, the rate of superoxide production was evaluated by photographing the same cell field at sequential time points under room temperature.

Evaluation of neuronal death. Death of cultured neurons was quantified by the propidium iodide method 20–24 hours after GD/GR (55). Propidium iodide–stained neurons were counted in 4 randomly selected fields of each well by an observer blinded to the experimental protocol and expressed as percentage of the total number of neurons in each well. Neuronal death after HG in vivo was evaluated after a 7-day survival period. Brain sections were stained by H&E staining or by the Fluoro-Jade B method (Histo-Chem Inc.), which gave comparable results (16, 61). Five coronal sections were collected from each animal, spaced 80 μm apart and spanning the hippocampus. An observer blinded to the experimental protocol counted the total number of eosinophilic or Fluoro-Jade B–stained neurons in each structure of interest, in both hemispheres. Data from each animal were expressed as the mean number of degenerating neurons per structure of interest.

In vitro Zn^{2+} detection. Cultures were loaded with 50 μM FluoZin-3 AM (Invitrogen) for 30 minutes, then subjected to GD or GD/GR. At indicated time points, cultures were photographed under uniform conditions with an inverted fluorescence microscope, using 490 nm excitation and a 535/25-nm band pass filter (40). Randomly selected photographic fields were digitized, and the mean fluorescence intensity of neuronal cell bodies was measured. The values for each neuron were averaged within each well and corrected for background fluorescence.

In vivo Zn^{2+} translocation. Vesicular and intracellular free zinc was imaged using the TSQ method (43). Rats were euthanized immediately after the designated treatments, and the fresh frozen brains were coronally sectioned. Five evenly spaced sections were collected through the hippocampal region of each brain and immersed in a solution of 4.5 μM TSQ (Molecular Probes; Invitrogen), 140 mM sodium barbital, and 140 mM sodium acetate (pH 10.5–11) for 60 seconds, then rinsed for 60 seconds in 150 mM NaCl. TSQ-zinc binding was imaged and photographed with a fluorescence microscope with 360 nm UV light and a 500-nm-long pass filter. The mean fluorescence intensity within the mossy fiber terminal area was measured and expressed as arbitrary intensity after subtraction of background fluorescence as measured in the lateral ventricle. Measurements from the 5 sections were averaged for each experimental group. Zinc levels in postsynaptic hippocampal CA1 neurons were evaluated in the same manner.

Statistics. Data are expressed as mean + SEM. Measurements of Et and TSQ fluorescence intensities were evaluated with the Kruskal-Wallis test and Dunn's test for comparisons between multiple groups. All other data were assessed by 1-way ANOVA followed by either the Tukey-Kramer test for multiple comparisons between groups or the Dunnett's test for comparisons of multiple groups against a common control group. *P* values of less than 0.05 were considered significant.

Acknowledgments

This work was supported by the Juvenile Diabetes Research Foundation (2-2006-113 to S.W. Suh), the NIH (NS051855 to R.A. Swanson and P50 NS14543 to P.H. Chan), and the Department of Veterans Affairs. We thank David McKinney for technical assistance, Carl Grunfelf and Kakha Artsivadze for helpful discussions, and Midori Yenari and Stephen Massa for critical reading of the manuscript.

Received for publication August 16, 2006, and accepted in revised form January 30, 2007.

Address correspondence to: Raymond A. Swanson, (127) Neurology, Veterans Affairs Medical Center, 4150 Clement Street, San Francisco, California 94121, USA. Phone: (415) 750-2011; Fax: (415) 750-2273; E-mail: raymond.swanson@ucsf.edu.

1. Davis, E.A., Keating, B., Byrne, G.C., Russell, M., and Jones, T.W. 1998. Impact of improved glycaemic control on rates of hypoglycaemia in insulin dependent diabetes mellitus. *Arch. Dis. Child.* **78**:111–115.
2. Seltzer, H.S. 1989. Drug-induced hypoglycemia. A review of 1418 cases. *Endocrinol. Metab. Clin. North Am.* **18**:163–183.
3. McCrimmon, R.J., and Frier, B.M. 1994. Hypoglycaemia, the most feared complication of insulin therapy. *Diabete. Metab.* **20**:503–512.
4. Auer, R.N. 1986. Progress review: hypoglycemic brain damage. *Stroke.* **17**:699–708.
5. Ben-Ami, H., Nagachandran, P., Mendelson, A., and Edoute, Y. 1999. Drug-induced hypoglycemic coma in 102 diabetic patients. *Arch. Intern. Med.* **159**:281–284.
6. Auer, R.N., Hugh, J., Cosgrove, E., and Curry, B. 1989. Neuropathologic findings in three cases of profound hypoglycemia. *Clin. Neuropathol.* **8**:63–68.
7. Auer, R.N., and Siesjo, B.K. 1993. Hypoglycaemia: brain neurochemistry and neuropathology. *Baillieres Clin. Endocrinol. Metab.* **7**:611–625.
8. Patrick, A.W., and Campbell, I.W. 1990. Fatal hypoglycaemia in insulin-treated diabetes mellitus: clinical features and neuropathological changes. *Diabet. Med.* **7**:349–354.
9. Kalimo, H., and Olsson, Y. 1980. Effects of severe hypoglycemia on the human brain. Neuropathological case reports. *Acta. Neurol. Scand.* **62**:345–356.
10. Nellgard, B., and Wieloch, T. 1992. Cerebral protection by AMPA- and NMDA-receptor antagonists administered after severe insulin-induced hypoglycemia. *Exp. Brain Res.* **92**:259–266.
11. Sandberg, M., Butcher, S.P., and Hagberg, H. 1986. Extracellular overflow of neuroactive amino acids during severe insulin-induced hypoglycemia: in vivo dialysis of the rat hippocampus. *J. Neurochem.* **47**:178–184.
12. Wieloch, T. 1985. Hypoglycemia-induced neuronal damage prevented by an N-methyl-D-aspartate antagonist. *Science.* **230**:681–683.
13. Patockova, J., et al. 2003. Oxidative stress in the brain tissue of laboratory mice with acute post insulin hypoglycemia. *Physiol. Res.* **52**:131–135.
14. Singh, P., Jain, A., and Kaur, G. 2004. Impact of hypoglycemia and diabetes on CNS: correlation of mitochondrial oxidative stress with DNA damage. *Mol. Cell. Biochem.* **260**:153–159.
15. Suh, S.W., Garnier, P., Aoyama, K., Chen, Y., and Swanson, R.A. 2004. Zinc release contributes to hypoglycemia-induced neuronal death. *Neurobiol. Dis.* **16**:538–545.
16. Suh, S.W., et al. 2003. Hypoglycemic neuronal death and cognitive impairment are prevented by poly(ADP-ribose) polymerase inhibitors administered after hypoglycemia. *J. Neurosci.* **23**:10681–10690.
17. Suh, S.W., Aoyama, K., Matsumori, Y., Liu, J., and Swanson, R.A. 2005. Pyruvate administered after severe hypoglycemia reduces neuronal death and cognitive impairment. *Diabetes.* **54**:1452–1458.
18. Ferrand-Drake, M., Friberg, H., and Wieloch, T. 1999. Mitochondrial permeability transition induced DNA-fragmentation in the rat hippocampus following hypoglycemia. *Neuroscience.* **90**:1325–1338.
19. Friberg, H., Ferrand-Drake, M., Bengtsson, F., Halestrap, A.P., and Wieloch, T. 1998. Cyclosporin A, but not FK 506, protects mitochondria and neurons against hypoglycemic damage and implicates the mitochondrial permeability transition in cell death. *J. Neurosci.* **18**:5151–5159.
20. Chinopoulos, C., and Adam-Vizi, V. 2006. Calcium, mitochondria and oxidative stress in neuronal pathology. Novel aspects of an enduring theme. *FEBS J.* **273**:433–450.
21. McGowan, J.E., Chen, L., Gao, D., Trush, M., and Wei, C. 2006. Increased mitochondrial reactive oxygen species production in newborn brain during hypoglycemia. *Neurosci. Lett.* **399**:111–114.
22. Decoursey, T.E., and Ligeti, E. 2005. Regulation and termination of NADPH oxidase activity. *Cell. Mol. Life Sci.* **62**:2173–2193.
23. Serrano, F., Kolluri, N.S., Wientjes, F.B., Card, J.P., and Klann, E. 2003. NADPH oxidase immunoreactivity in the mouse brain. *Brain Res.* **988**:193–198.
24. Tejada-Simon, M.V., et al. 2005. Synaptic localization of a functional NADPH oxidase in the mouse hippocampus. *Mol. Cell. Neurosci.* **29**:97–106.
25. Vallet, P., et al. 2005. Neuronal expression of the NADPH oxidase NOX4, and its regulation in mouse experimental brain ischemia. *Neuroscience.* **132**:233–238.
26. Rhee, S.G. 2006. Cell signaling. H2O2, a necessary evil for cell signaling. *Science.* **312**:1882–1883.
27. Kim, Y.H., and Koh, J.Y. 2002. The role of NADPH oxidase and neuronal nitric oxide synthase in zinc-induced poly(ADP-ribose) polymerase activation and cell death in cortical culture. *Exp. Neurol.* **177**:407–418.
28. Murakami, K., et al. 1998. Mitochondrial susceptibility to oxidative stress exacerbates cerebral infarction that follows permanent focal cerebral ischemia in mutant mice with manganese superoxide dismutase deficiency. *J. Neurosci.* **18**:205–213.
29. Zhao, H., et al. 2003. Superoxide reacts with hydroethidine but forms a fluorescent product that is distinctly different from ethidium: potential implications in intracellular fluorescence detection of superoxide. *Free Radic. Biol. Med.* **34**:1359–1368.
30. Chan, P.H., et al. 1998. Overexpression of SOD1 in transgenic rats protects vulnerable neurons against ischemic damage after global cerebral ischemia and reperfusion. *J. Neurosci.* **18**:8292–8299.
31. Dugan, L.L., et al. 1995. Mitochondrial production of reactive oxygen species in cortical neurons following exposure to N-methyl-D-aspartate. *J. Neurosci.* **15**:6377–6388.
32. Nishikawa, T., et al. 2000. Normalizing mitochondrial superoxide production blocks three pathways of hyperglycaemic damage. *Nature.* **404**:787–790.
33. Starkov, A.A., et al. 2004. Mitochondrial alpha-ketoglutarate dehydrogenase complex generates reactive oxygen species. *J. Neurosci.* **24**:7779–7788.
34. Gupte, S.A., et al. 2005. Cytosolic NADPH may regulate differences in basal Nox oxidase-derived superoxide generation in bovine coronary and pulmonary arteries. *Am. J. Physiol. Heart Circ. Physiol.* **288**:H13–H21.
35. Simons, J.M., Hart, B.A., Ip Vai Ching, T.R., Van Dijk, H., and Labadie, R.P. 1990. Metabolic activation of natural phenols into selective oxidative burst agonists by activated human neutrophils. *Free Radic. Biol. Med.* **8**:251–258.
36. Groemping, Y., and Rittinger, K. 2005. Activation and assembly of the NADPH oxidase: a structural perspective. *Biochem. J.* **386**:401–416.
37. Inanami, O., et al. 1998. Activation of the leukocyte NADPH oxidase by phorbol ester requires the phosphorylation of p47PHOX on serine 303 or 304. *J. Biol. Chem.* **273**:9539–9543.
38. He, L., et al. 2005. Effect of p47phox gene deletion on ROS production and oxygen sensing in mouse carotid body chemoreceptor cells. *Am. J. Physiol. Lung Cell. Mol. Physiol.* **289**:L916–L924.
39. Noh, K.M., and Koh, J.Y. 2000. Induction and activation by zinc of NADPH oxidase in cultured cortical neurons and astrocytes. *J. Neurosci.* **20**:RC111.
40. Devinney, M.J., 2nd, Reynolds, I.J., and Dineley, K.E. 2005. Simultaneous detection of intracellular free calcium and zinc using fura-2FF and FluoZin-3. *Cell Calcium.* **37**:225–232.
41. Koh, J.Y., et al. 1996. The role of zinc in selective neuronal death after transient global cerebral ischemia. *Science.* **272**:1013–1016.
42. Frederickson, C.J. 1989. Neurobiology of zinc and zinc-containing neurons. *Int. Rev. Neurobiol.* **31**:145–238.
43. Frederickson, C.J., Kasarskis, E.J., Ringo, D., and Frederickson, R.E. 1987. A quinoline fluorescence method for visualizing and assaying the histochemically reactive zinc (bouton zinc) in the brain. *J. Neurosci. Methods.* **20**:91–103.
44. Kohler, E., Barrach, H., and Neubert, D. 1970. Inhibition of NADP dependent oxidoreductases by the 6-aminonicotinamide analogue of NADP. *FEBS Lett.* **6**:225–228.
45. de Courten-Myers, G.M., et al. 2000. Hypoglycemic brain injury: potentiation from respiratory depression and injury aggravation from hyperglycemic treatment overshoots. *J. Cereb. Blood Flow Metab.* **20**:82–92.
46. Malouf, R., and Brust, J.C. 1985. Hypoglycemia: causes, neurological manifestations, and outcome. *Ann. Neurol.* **17**:421–430.
47. Choi, I.Y., Lee, S.P., Kim, S.G., and Gruetter, R. 2001. In vivo measurements of brain glucose transport using the reversible Michaelis-Menten model and simultaneous measurements of cerebral blood flow changes during hypoglycemia. *J. Cereb. Blood Flow Metab.* **21**:653–663.
48. Adler, P.M. 1986. Serum glucose changes after administration of 50% dextrose solution: pre- and in-hospital calculations. *Am. J. Emerg. Med.* **4**:504–506.
49. Chan, P.H. 2001. Reactive oxygen radicals in signaling and damage in the ischemic brain. *J. Cereb. Blood Flow Metab.* **21**:2–14.
50. Stolk, J., Hiltermann, T.J., Dijkman, J.H., and Verhoeven, A.J. 1994. Characteristics of the inhibition of NADPH oxidase activation in neutrophils by apocynin, a methoxy-substituted catechol. *Am. J. Respir. Cell Mol. Biol.* **11**:95–102.
51. Dodd, O.J., and Pearse, D.B. 2000. Effect of the NADPH oxidase inhibitor apocynin on ischemia-reperfusion lung injury. *Am. J. Physiol. Heart Circ. Physiol.* **279**:H303–H312.
52. Frederickson, C.J., Koh, J.Y., and Bush, A.I. 2005. The neurobiology of zinc in health and disease. *Nat. Rev. Neurosci.* **6**:449–462.
53. Frederickson, C.J., et al. 2002. Depletion of intracellular zinc from neurons by use of an extracellular chelator in vivo and in vitro. *J. Histochem. Cytochem.* **50**:1659–1662.
54. Beaulieu, C., Dyck, R., and Cynader, M. 1992. Enrichment of glutamate in zinc-containing terminals of the cat visual cortex. *Neuroreport.* **3**:861–864.
55. Ying, W., Han, S.K., Miller, J.W., and Swanson, R.A. 1999. Acidosis potentiates oxidative neuronal death by multiple mechanisms. *J. Neurochem.* **73**:1549–1556.
56. Kauppinen, T.M., and Swanson, R.A. 2005. Poly(ADP-ribose) polymerase-1 promotes microglial activation, proliferation, and matrix metalloproteinase-9-mediated neuron death. *J. Immunol.* **174**:2288–2296.
57. Auer, R.N., Olsson, Y., and Siesjo, B.K. 1984. Hypoglycemic brain injury in the rat. Correlation of density of brain damage with the EEG isoelectric time: a quantitative study. *Diabetes.* **33**:1090–1098.
58. Schachter, M. 1951. Hexamethonium and insulin hypoglycaemia. *J. Physiol.* **115**:206–209.
59. Suh, S.W., et al. 2000. Evidence that synaptically-released zinc contributes to neuronal injury after traumatic brain injury. *Brain Res.* **852**:268–273.
60. Budd, S.L., Castilho, R.F., and Nicholls, D.G. 1997. Mitochondrial membrane potential and hydroethidine-monitored superoxide generation in cultured cerebellar granule cells. *FEBS Lett.* **415**:21–24.
61. Schmued, L.C., and Hopkins, K.J. 2000. Fluorojade B: a high affinity fluorescent marker for the localization of neuronal degeneration. *Brain Res.* **874**:123–130.